Available online at www.sciencedirect.com
SCIENCE DIRECT®
Journal of Molecular Catalysis A: Chemical 219 (2004) 155–164
JOURNAL OF MOLECULAR CATALYSIS A: CHEMICAL
www.elsevier.com/locate/molcata

Characterization of copper oxide supported on ceria-modified anatase

Haiyang Zhu [a], Mingmin Shen [a], Yan Kong [a], Jianming Hong [b], Yuhai Hu [a], Tiandong Liu [a], Lin Dong [a,*], Yi Chen [a], Can Jian [c], Zhong Liu [c]

[a] *Key Laboratory for Mesoscopic Chemistry, Department of Chemistry, College of Chemistry and Chemical Engineering, Nanjing University, Nanjing 210093, PR China*
[b] *Center of Modern Analysis, Nanjing University, Nanjing 210093, PR China*
[c] *Department of Chemistry and Environment, Tibet University, Lhasa 850000, China*

Received 30 December 2003; received in revised form 30 April 2004; accepted 30 April 2004

Available online 7 June 2004

Abstract

XRD, LRS, XPS, TPR and ESR have been used to investigate the dispersion and reduction behavior of copper oxide in $CuO/CeO_2/TiO_2$ samples (copper oxide supported on ceria-modified anatase). The results indicate that: (1) ceria can be highly dispersed on the surface of TiO_2 support, and corresponding to a dispersion capacity (DC) of about 6.98 Ce^{4+} ions/nm^2 TiO_2; (2) the dispersion of copper oxide on ceria-modified TiO_2 is below the loading amount of ceria. For the samples with ceria loading prior to 6.98 Ce^{4+} ions/nm^2 TiO_2, the dispersion of copper oxide decreases with the ceria loading. When the loading of ceria is greater than 6.98 Ce^{4+} ions/nm^2 TiO_2, the dispersion of copper oxide increases with ceria loading; (3) the reduction behavior of the copper oxide species are also shown to be correlated to the ceria loading. For $CuO/CeO_2/TiO_2$ samples with the low ceria loading of 3 wt.%, the dispersed copper oxide species could be simply regarded as two species (Cu–I and Cu–II) according to the differences in the reduction behavior. For the high ceria loading $CuO/CeO_2/TiO_2$ samples, e.g. ceria loading amount of 40 wt.%, the TPR profiles indicate that the reduction behavior of copper oxide is similar to that in CuO/CeO_2 system, and the sample should be approximately regarded as the composition of two systems, CuO/CeO_2 and CeO_2/TiO_2. In addition, the activities of the catalysts, CuO/TiO_2, $CuO/CeO_2/TiO_2$ and CuO/CeO_2, in the NO + CO reaction at different temperatures have been studied to monitor the relationship between the catalytic activity versus the composition of the catalysts. For the samples with low copper oxide loading, the catalytic activity varies as in this order: 4Cu–6Ce–Ti $<$ CuO/TiO_2 $<$ CuO/CeO_2 $\approx$ 4Cu–40Ce–Ti, which suggests that the dispersed ceria species hinder the activity of surface copper species in 4Cu–6Ce–Ti sample. While for the samples with high ceria loading, the activities of copper species are greatly enhanced due to the formation of crystalline CeO_2. Furthermore, for the $CuO/CeO_2/TiO_2$ samples, especially for that with lower copper oxide and ceria loadings, the dispersion states of the copper and ceria are also discussed by the consideration of incorporation model proposed previously [Catal. Lett. 12 (1992) 51].

Keywords: Anatase; Copper oxide species; Ceria; Dispersion capacity (DC); NO + CO

1. Introduction

Supported metal oxides are extensively used as heterogeneous catalysts in numerous chemical processes, e.g. ranging from hydrodesulfurization, cracking, polymerization, and partial oxidation of hydrocarbons to the selective reduction of nitrogen oxides. It is well established that the supported metal oxide species might have a variety of structures strongly depending on the experimental conditions such as the loading amount of the oxide and the calcination temperature. Accordingly, a large number of studies have been devoted to exploring the interaction between the support and the dispersed oxide species, and various explanations or models concerning the nature of the interaction have been proposed [1–7].

Titanium oxide is one of the major supports widely applied in heterogeneous catalysis [8], and it has been found that the catalytic activity of HDS catalyst can be improved by choosing titanium oxide instead of γ-Al_2O_3 as the support [9,10]. In recent years, TiO_2, as a support,

* Corresponding author. Tel.: +86-25-83594945; fax: +86-25-83317761.
E-mail address: chem718@nju.edu.cn (L. Dong).

1381-1169/$ – see front matter © 2004 Elsevier B.V. All rights reserved.
doi:10.1016/j.molcata.2004.04.032

has been widely used in heterogeneous catalysts, especially in photo-catalysis. It is well known that transition metal oxides supported on TiO_2 have been employed in various important reactions, for examples, V_2O_5/TiO_2 in the selective catalytic reduction of NO_x with NH_3 and the oxidation of sulfur dioxide to sulfur trioxide; MoO_3/TiO_2 in the selective photo-oxidation of alcohol; and $CoO–MoO_3/TiO_2$ in hydrodesulfurization of hydrocarbon oils, etc. [8,11–14]. Ceria has proved to be a very important and potential component in the three-way catalysts (TWCs), and been widely investigated for the past few years. However, it is an arduous task to define the role of the ceria in the catalysis since multiple effects have been attributed to this promoter [15], which include: promoting the noble metal dispersion; increasing the thermal stability of the γ-Al_2O_3 support; promoting the water gas shift (WGS) and steam reforming reactions; favoring catalytic activity at the interfacial metal-support sites, promoting CO removal through oxidation employing lattice oxygen; storing and releasing oxygen under, respectively, lean and rich conditions.

The catalysts containing transition metals, especially copper, show a potential application for the treatment of exhaust gas from automobiles [16–19], and special attention has also been paid to this system as a substitute for noble metal containing catalysts recently [20]. Generally, three forms of the copper containing catalysts have been used for the investigations, e.g. unsupported copper oxide catalysts [21], supported copper oxide catalysts and supported metal copper catalysts [22,23]. As reported by Andersson and co-workers, the dispersed copper oxide on TiO_2 was active for the complete oxidation of CO and toluene. However, the presence of copper oxide species accelerates the sintering of TiO_2 support, which prohibits the application of this catalyst [24]. Further study indicated that, doping a certain amount of ceria in CuO/TiO_2 greatly promoted the activity of CO oxidation and enhanced the stabilization of this catalyst [25]. As documented in the literature, for the CuO/TiO_2 sorbent, both uptake rates and capacity of NO_x significantly increase as ceria species is doped [26].

Despite the studies on the Cu–Ce–Ti–O catalysts mentioned above, the role of the doped species and the nature of the interactions among the doped species and the active species, as well as the support, have not been solved.

In present work, the studies have been mainly focused on attempting to [1] determine the dispersion capacity (DC) and surface states of ceria on TiO_2, [2] investigate the influence of the ceria loading amounts to the dispersion of copper oxide in the $CuO/CeO_2/TiO_2$ catalysts, [3] explore the relationship between the catalytic activity for NO + CO reaction versus composition of the $CuO/CeO_2/TiO_2$ catalysts. The results have shown that the dispersion of CuO and ceria, the surface states of the supported binary oxide samples, as well as the catalytic properties in "CO + NO" reaction are strongly dependent on the loading amount of the individual oxides.

2. Experimental

TiO_2 support was prepared via hydrolysis of titanium alkoxides, the product was washed, dried and then calcined in flowing air at 500 °C for 5 h. The anatase crystalline form of the product was identified by XRD [27], and the BET surface area is 83 $m^2\,g^{-1}$.

CeO_2/TiO_2 (ceria-modified TiO_2) was prepared by impregnating TiO_2 with an aqueous solution of cerious nitrate followed by drying at 100 °C overnight and then calcined in flowing air at 500 °C for 7 h.

$CuO/CeO_2/TiO_2$ samples were prepared by impregnating CeO_2/TiO_2 with an aqueous solution of cupric nitrate followed by drying at 100 °C overnight and then calcined in flowing air at 500 °C for 7 h. For the sake of simplicity, $CuO/CeO_2/TiO_2$ samples were noted as *x*Cu–*y*Ce–Ti, e.g. 4Cu–3Ce–Ti corresponds to the sample with copper oxide and ceria loading amount of 4 and 3 wt.% respectively. The results of BET surface area of ceria-modified TiO_2 suggest that the change of support surface area could be neglected in this system, which is consistent to the results reported in the literature [7].

X-ray diffraction (XRD) patterns were obtained with a Shimadzu XD-3A diffractometer employing Ni-filtered Cu Kα radiation (0.15418 nm). The X-ray tube was operated at 35 kV and 15 mA. Quantitative XRD methods used in this work are described elsewhere [28].

Fourier transform laser Raman spectra (FT-LRS) were recorded on a Bruker RFS-100 Fourier transform spectrometer with an InGaAs detector cooled by liquid nitrogen. Raman excitation at 1064 nm was provided by a Nd-YAG laser. The laser power measured at the powder sample (∼30 mg) was 100 mW, and spectra were accumulated for 50 scans at 4 cm^{-1} resolutions in back-scattering geometry.

X-ray photoelectron spectroscopy (XPS) results were obtained by using a V.G. Escalab MK II spectrometer equipped with a hemispherical electron analyzer. The system was operated at 13 kV and 20 mA using a magnesium anode (Mg Kα, $E = 1253.6$ eV). A binding energy (BE) of 284.5 eV for the C 1s level was used as an internal reference.

Electron spin resonance (ESR) spectra were recorded on a Bruker electron spinning resonance spectrometer (EMX EPR spectrometer) at room temperature. Before the determination, the catalysts were put into a glass tube, and then calcined in air at 300 °C for 3 h.

Temperature-programmed reduction (TPR) was carried out in a quartz U-tube reactor, and 30 mg sample was used for each measurement. Prior to the reduction, the sample was pretreated in an air stream at 100 °C for 1 h and then cooled to room temperature. After that, H_2–Ar mixture (7% H_2 by volume) was switched on and the temperature was increased linearly at a rate of 10 °C min^{-1}. A thermal conductivity cell detected the consumption of H_2 in the reactant stream. Before each measurement, a TPR profile of CuO (5 mg) was also obtained as a reference for the calculations.

The activities of the catalysts for NO + CO reaction were measured under steady state, using a feed stream with a fixed composition, NO 3.33%, CO 6.67% and He 90% by volume as diluent. A quartz tube was employed as the reactor and the requisite quantity of catalysts (100 mg for each test) was used. The catalysts were pretreated in N_2 stream at 100 °C for 1 h and then heated to reaction temperature, after that, the mixed gases were switched on. The reactions were carried out at different temperatures with the same space velocity of 6000 ml g^{-1} h^{-1}. Two columns and thermal conductivity detector (TCD) were used for the purpose of analyzing the production, column A was Porapak Q used for separating N_2O and CO_2, and column B was 13X molecular sieve (30–60 M) used for separating N_2, NO and CO.

3. Results and discussion

3.1. Dispersion of ceria on TiO_2

Fig. 1 shows the XRD patterns of a series of CeO_2/TiO_2 samples with different ceria loading amounts. For the samples with ceria loading amounts <16 wt.%, there are no typical diffraction peaks of crystalline CeO_2 in the patterns, except those of TiO_2 supports. However, as the ceria loading amounts are increased from 16 to 30 wt.%, the characteristic peaks corresponding to crystalline CeO_2 (centered at $2\theta = 28.40^\circ$) are observed, which means that crystalline CeO_2 has formed in these samples besides the dispersed ceria. An XRD quantitative analysis method was employed to determine the dispersion capacity of ceria on TiO_2 support [27,28], and the results indicated that the DC of ceria is about 14.64 wt.%, i.e. 7.23 Ce^{4+} ions/nm^2 TiO_2, as shown in Fig. 2.

LRS results of a series of CeO_2/TiO_2 samples with various ceria loading amounts are shown in Fig. 3. TiO_2 support presents several Raman peaks centered at 144.3, 395.7, 519.4 and 642.1 cm^{-1}. For the samples with ceria loading amounts of 8 and 10 wt.%, only Raman peaks of TiO_2 support are observed, while as the ceria loading amounts reached 16 wt.%, the characteristic Raman peaks of crystalline CeO_2 at 464 cm^{-1} appeared, as shown in Fig. 3(c)–(f).

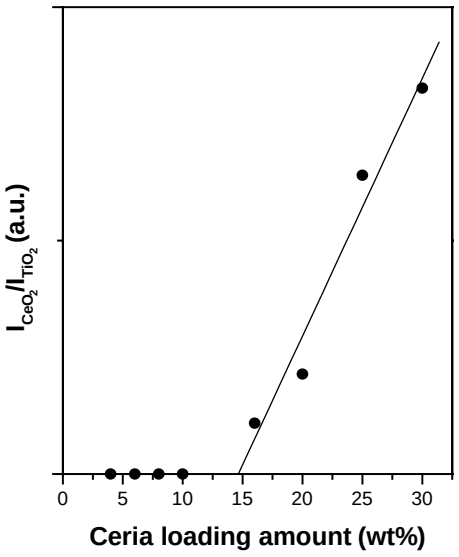

Fig. 2. Quantitative XRD result of CeO_2/TiO_2 samples.

Fig. 4 shows the relationship between Raman intensity ratio and ceria loading, e.g. I_{CeO_2} (462.5 cm^{-1})/I_{TiO_2} (144.3 cm^{-1}). It can be seen that the DC of ceria on TiO_2 from Raman results is about 13.80 wt.%, i.e. 6.75 Ce^{4+} ions/nm^2 TiO_2, which is close to that from XRD.

As discussed previously [27,29], the (0 0 1) plane of the TiO_2 (anatase) is considered the preferentially exposed plane, and the dispersion capacity and the surface states of

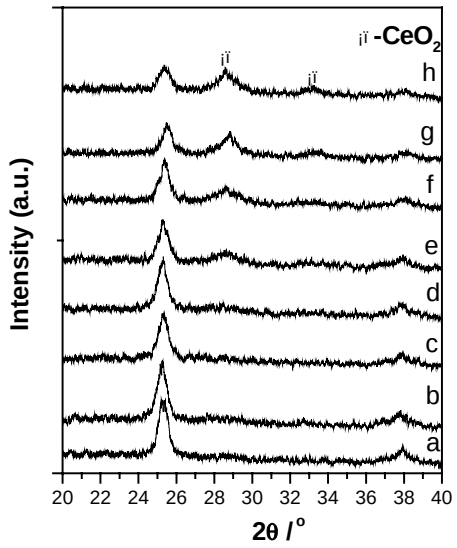

Fig. 1. XRD patterns: (a–h) for CeO_2/TiO_2 samples with ceria loading amounts of 4, 6, 8, 10, 16, 20, 25, and 30 wt.%, respectively.

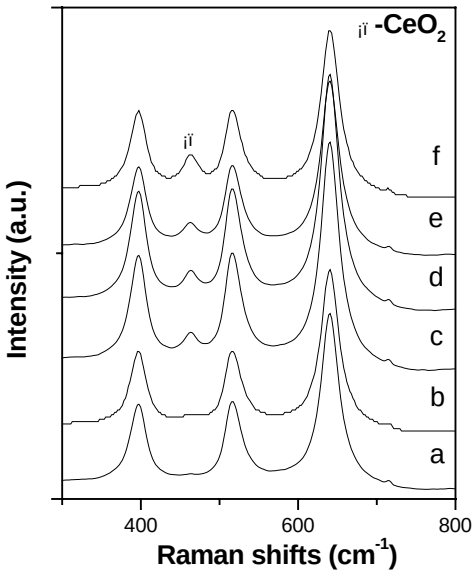

Fig. 3. Raman results: (a–f) for CeO_2/TiO_2 samples with ceria loading amounts of 8, 10, 16, 20, 25 and 30 wt.%, respectively.

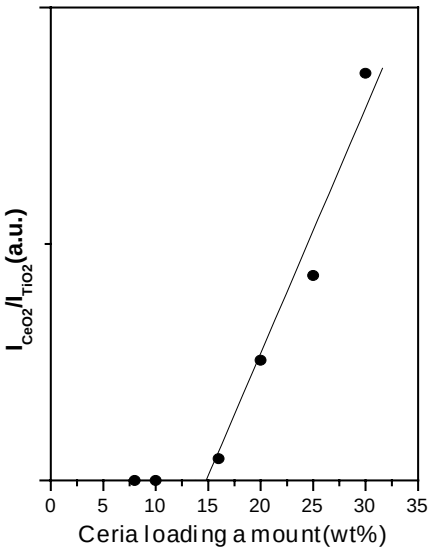

Fig. 4. Quantitative Raman results of CeO_2/TiO_2 samples.

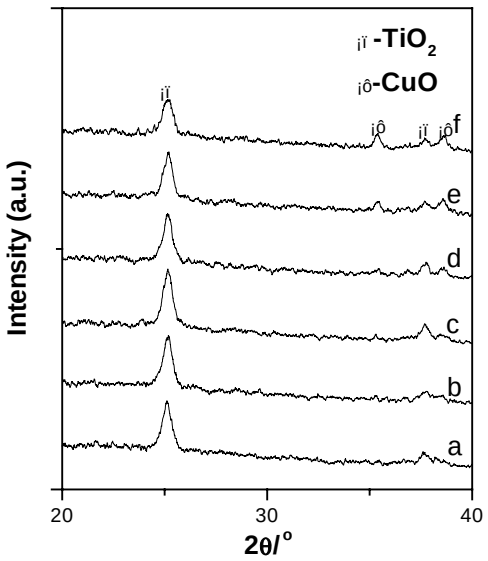

Fig. 6. XRD patterns: (a–f) for *x*Cu–3Ce–Ti samples with copper oxide loading amounts of 4, 6, 8, 12, 16 and 20 wt.%, respectively.

the active species could be expected by considering the surface structure of TiO_2. For anatase, the vacant site density in (0 0 1) plane is about 6.98 sites/nm^2, shown in Fig. 5(a). When ceria is dispersed on the surface of TiO_2, Ce^{4+} may occupy the surface vacant site on TiO_2, and the two accompanying oxygen anions will stay at the top of the occupied site as capping oxygen, compensating the extra positive charge. Consequently, the DC of ceria species is expected about to be 6.98 Ce^{4+} ions/nm^2 TiO_2, i.e. 14.27 wt.%, which is basically in agreement with the XRD and Raman results. The surface structure of the dispersed ceria species could be tentatively shown as in Fig. 5(b).

3.2. Dispersion of CuO on CeO_2/TiO_2 support

To investigate the variation of the dispersion of copper oxide with the addition of different ceria loadings in TiO_2 support, the ceria-modified TiO_2 supports, 3Ce–TiO_2, 6Ce–TiO_2, 20Ce–TiO_2 and 40Ce–TiO_2, were used to support copper oxide. Figs. 6 and 7 show the XRD patterns of *x*Cu–3Ce–Ti and *x*Cu–40Ce–Ti, i.e. the lower and higher ceria-containing samples were used as the examples, respectively. In Fig. 6, no crystalline CeO_2 formed in the *x*Cu–3Ce–Ti samples according to the absence of the typical diffraction peaks representing crystalline CeO_2, and the typical peaks of crystalline CuO appear for the samples with copper oxide loading amounts beyond 6 wt.%, which indicates that crystalline CuO formed in these samples. In Fig. 7, a strong diffraction peak of CeO_2 appears in all of the *x*Cu–40Ce–Ti samples, and the peaks of crystalline CuO can be clearly seen as copper oxide loading amount is higher than 6 wt.% and the peak intensities of CuO also increase with the copper loading. The results suggest that crystalline ceria formed in all the *x*Cu–40Ce–Ti samples, and the ceria and ceria-modified TiO_2 will be the supports for the dispersion of copper oxide simultaneously.

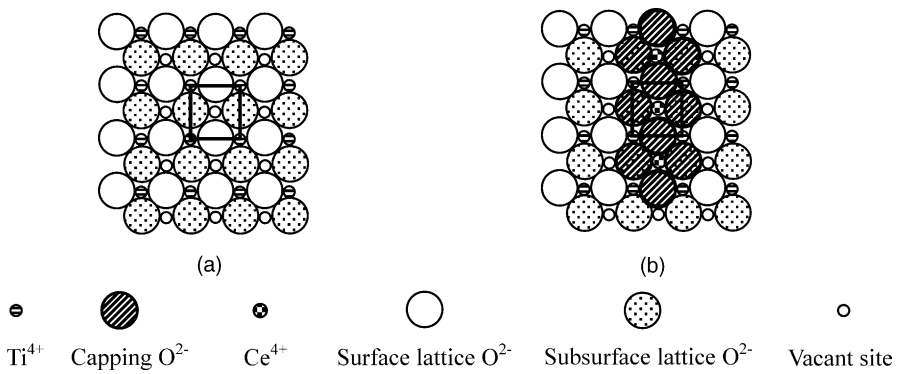

Fig. 5. The schematic diagram for the incorporated Ce^{4+} ions in the surface vacant sites on the (0 0 1) plane of TiO_2 (anatase): (a) (0 0 1) plane of TiO_2 (anatase); (b) incorporation of the dispersed Ce^{4+} species on the (0 0 1) plane of TiO_2 (anatase) support.

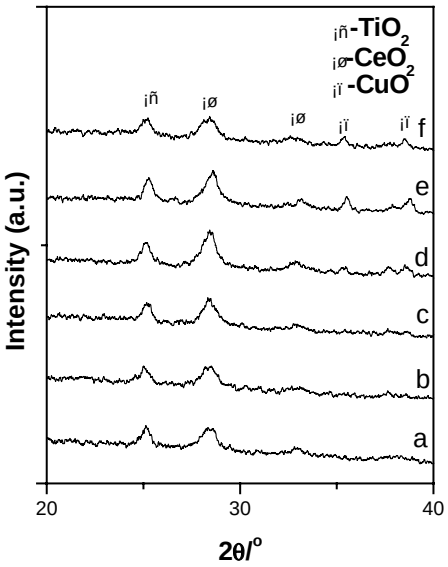

Fig. 7. XRD patterns: (a–f) for *x*Cu–40Ce–Ti samples with copper oxide loading of 4, 6, 8, 12, 16 and 20 wt.%, respectively.

Quantitative XRD analysis of the dispersion of copper oxide on ceria-modified TiO_2 is shown in Fig. 8. The results indicate that the dispersion of copper oxide is relative to the ceria loading amounts. When the loading amounts of ceria are ranging from 3 to 6 wt.%, the dispersion of copper oxide decreases, but as the loading amounts of ceria increase from 20 to 40 wt.%, it increases slightly.

With consideration of the incorporation model proposed elsewhere [30], when the ceria loading amount is lower than the DC of ceria on TiO_2, the higher the ceria loading amount is, the less the available surface vacant sites of TiO_2 for copper oxide are. However, when the ceria loadings are highly beyond the DC, the surface vacant sites on TiO_2 support have been completely occupied by the Ce^{4+} ions in the dispersed ceria species, and copper oxide species would disperse on the surface of formed crystalline CeO_2. Along this line, it seems to suggest that, the decrease of the dispersion of copper oxide on the surface of ceria-modified TiO_2 support should be due to the occupation of the incorporated Ce^{4+} ions into the surface vacancies of TiO_2 support, and the increase of the dispersion of copper oxide might be, at least partly, attributed to the dispersion of copper oxide on the surface of the formed CeO_2 particles. As reported previously, copper oxide species can dispersed on the surface of CeO_2 with a DC of 6.98 ions/nm^2 CeO_2 [31]. The dispersion of copper oxide on ceria-modified TiO_2 supports with various ceria loading amounts is listed in Table 1.

Table 1
Dispersion of copper oxide on ceria-modified TiO_2 supports with various ceria loading amounts

Samples	Dispersion of copper oxide on supports (wt.%)
*x*Cu–3Ce–Ti	6.91
*x*Cu–6Ce–Ti	5.54
*x*Cu–20Ce–Ti	5.82
*x*Cu–40Ce–Ti	7.26

To get more understanding about the surface properties of Cu–Ce–Ti catalysts, XPS was used to characterize the samples: 4Cu–6Ce–Ti, CuO/CeO_2 (in which, 2.41 Cu^{2+} ions/nm^2 CeO_2) and CuO/TiO_2 (in which, 4.94 Cu^{2+} ions/nm^2 TiO_2). For the three samples, the copper oxide should exist in dispersion state, as reported elsewhere [27,31].

The Cu $2p_{3/2}$ binding energies in 4Cu–6Ce–Ti, CuO/TiO_2 and CuO/CeO_2 samples are 932.2, 931.9 and 932.2 eV, respectively, shown as in Fig. 9. It has been well established that for copper species the presence and absence of the shake-up peak are the characteristic for Cu^{2+} species and Cu^{+} species [32]. For CuO/TiO_2 and 4Cu–6Ce–Ti samples, a shake-up peak can be observed evidently, which indicates that Cu^{2+} species exist in these two samples. In contrast,

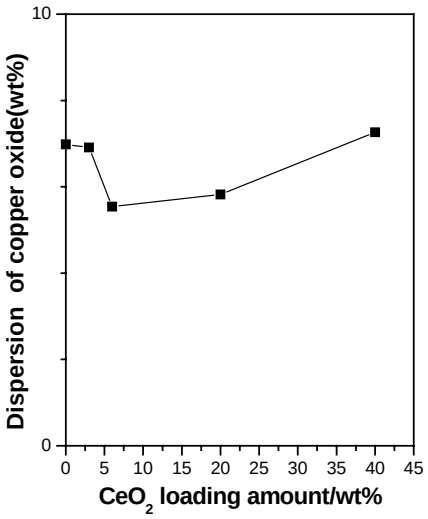

Fig. 8. Dispersion of copper oxide vs. ceria loading amounts.

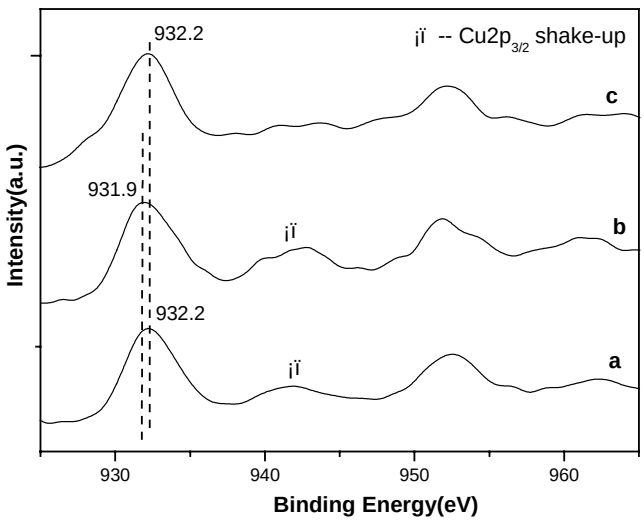

Fig. 9. Cu 2p XPS spectra: (a) 4Cu–6Ce–Ti; (b) CuO/TiO_2; (c) CuO/CeO_2.

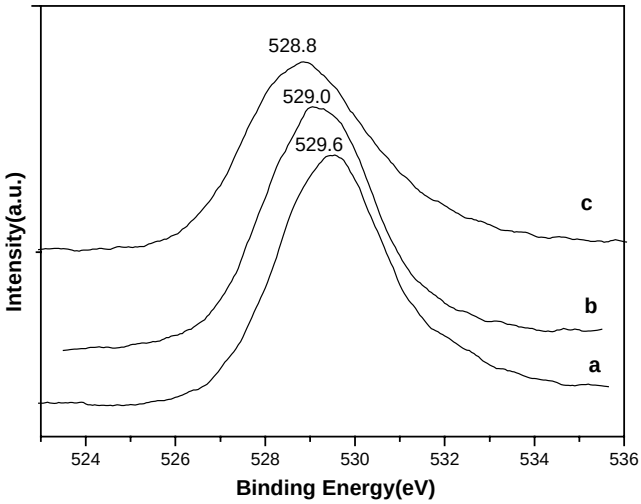

Fig. 10. O 1s XPS spectra: (a) CuO/TiO_2; (b) 4Cu–6Ce–Ti; (c) CuO/CeO_2.

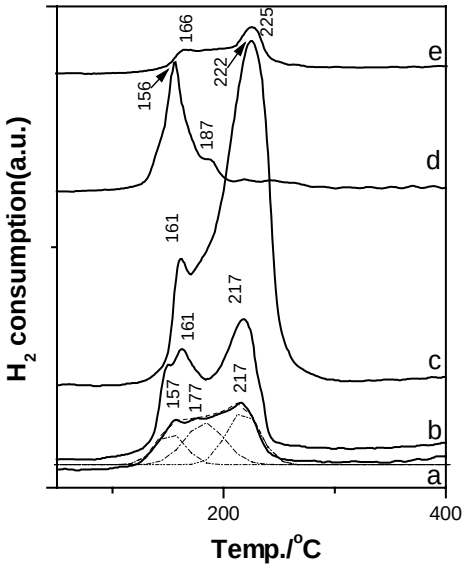

Fig. 11. TPR profiles of *x*Cu–3Ce–Ti samples: (a–c) with copper oxide loading amounts of 4, 8 and 16 wt.%, respectively; (d) CuO/CeO_2 sample with a copper oxide loading amount of 4 wt.%; (e) CuO/TiO_2 sample with a copper oxide loading amount of 4 wt.%.

for CuO/CeO_2 sample, almost no shake-up peak can be observed in Fig. 9(c), which suggests that copper species mainly exist as Cu^+ species. It seems possible that the reduction of Cu^{2+} to Cu^+ occurs under the procedure of XPS determination [25], and this should result from the properties of ceria with the oxygen storage and release capacity [15]. In addition, the intensity ratio of the shake-up to Cu $2p_{3/2}$ peak in 4Cu–6Ce–Ti sample is about 0.232, which is much smaller than that in CuO/TiO_2, i.e. 0.409, and this result seems to further support the suggestion that the reduction of copper oxide was resulted from the influence of ceria addition. In addition, the peaks at ca. 952 eV in these samples attributed to Cu $2p_{1/2}$ peak varies in the similar trends as Cu $2p_{3/2}$ peak.

Fig. 10 shows the O 1s XPS results of surface oxygen species in CuO/TiO_2, 4Cu–6Ce–Ti and CuO/CeO_2 samples, and the centers of O 1s binding energy are 529.6, 529.0 and 528.8 eV, respectively. For 4Cu–6Ce–Ti sample, doping of ceria leads to the BE value shift of O 1s between those of CuO/TiO_2 and CuO/CeO_2, which means that, in some extent, the properties of the surface oxygen species should be the common contribution of O–Cu, O–Ce and O–Ti contained. This result might suggest that, for the metal oxide catalysts design, the individual properties of O–M from the components included in the sample should be considered, especially for the selective oxidations reaction via surface crystallite oxygen.

3.3. Reduction behavior of copper oxide in $CuO/CeO_2/TiO_2$ samples

Figs. 11–13 show the TPR profiles of *x*Cu–3Ce–Ti, *x*Cu–6Ce–Ti and *x*Cu–40Ce–Ti samples respectively. In addition, the profiles of CuO/CeO_2 (4.76 Cu^{2+} ions/nm^2 CeO_2, less than the dispersion capacity of copper oxide in CuO/CeO_2 [31]) and CuO/TiO_2 (4.94 Cu^{2+} ions/nm^2 TiO_2) samples have also been employed for comparison, shown as in Fig. 11(d) and (e). Generally speaking, the shapes of TPR profiles varied with both the copper oxide and ceria loadings, which also indicated the complexity of the reduction process in these samples. To further approach the relationship between the amounts of various copper oxide species and their reduction behavior, a quantitative analysis has been tentatively employed in this section. For example, a quantitative treatment for the sample with 4Cu–3Ce–Ti has been shown in the dot line of Fig. 11(a), and the same treatment has been reported elsewhere [33–35]. The corresponding quantitative data for the samples are listed in Table 2.

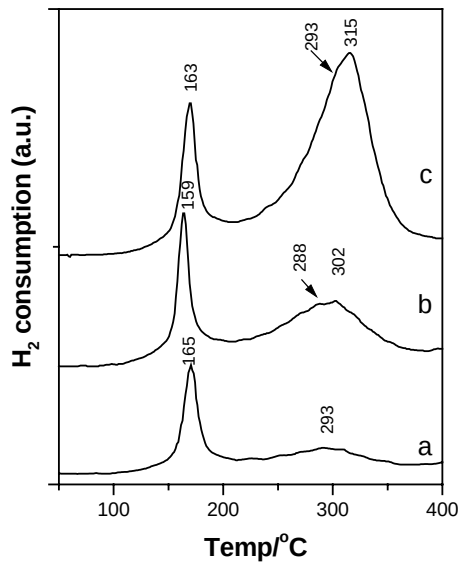

Fig. 12. TPR profiles of *x*Cu–6Ce–Ti samples: (a–c) with copper oxide loading amounts of 4, 8 and 16 wt.%, respectively.

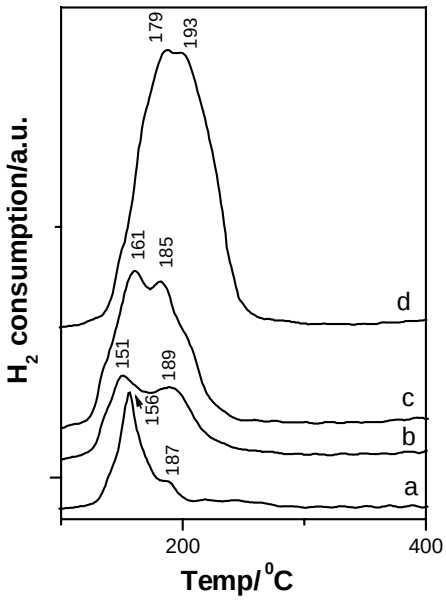

Fig. 13. TPR profiles: (a) CuO/CeO_2 sample with a copper oxide loading amount of 4 wt.%; *x*Cu–40Ce–Ti samples: (b–d) with copper oxide loading amounts of 4, 8 and 16 wt.%, respectively.

As shown in Fig. 11(a), the TPR profile of 4Cu–3Ce–Ti has a broad peak, which could be regarded as the contribution of three individual peaks centered at 157, 177 and 217 °C. Considering the TPR profile of CuO/TiO_2 sample, peak 177 °C should be ascribed to the reduction of highly dispersed copper oxide species on the surface of TiO_2, signed as Cu–I, i.e. Cu–Ti. Comparing the peak at 157 °C of 4Cu–3Ce–Ti and TPR profile of CuO/CeO_2 sample (Fig. 11(d)), it seems to suggest that this peak would be related to the reduction of the highly dispersed copper oxide species closely contacting with the dispersed ceria on TiO_2, which is signed as Cu–II, Ce–Cu–Ti. A possible scheme of the surface copper species in 4Cu–3Ce–Ti sample should be shown as in Fig. 14. As for the reduction peak at 217 °C, signed as Cu–III, it should be resulted from the reduction of CuO clusters in contact with TiO_2 surface [27,36].

Table 2
Amounts of copper oxide species in the *x*Cu–*y*Ce–Ti samples calculated by quantitative TPR

	Amount of copper oxide species (10^{-3} mmol Cu^{2+})			
	Cu–I	Cu–II	Cu–III	Cu–IV
4Cu–3Ce–Ti	4.97	5.46	5.79	0
8Cu–3Ce–Ti	5.16	10.29	8.68	6.34
16Cu–3Ce–Ti	6.13	12.56	17.56	25.14
4Cu–6Ce–Ti	0	9.12	6.71	0
8Cu–6Ce–Ti	0	9.03	9.65	7.68
16Cu–6Ce–Ti	0	9.21	21.31	29.29
4Cu–40Ce–Ti	1.82[a]	7.66[a]	11.82	0
8Cu–40Ce–Ti	5.21[a]	8.93[a]	21.80	2.70
16Cu–40Ce–Ti	1.73[a]	8.73[a]	19.74	50.45

[a] H_2 consumption of copper oxide species during stepwise reduction, and first row corresponds to reduction of Cu^{2+} to Cu^+, and second row corresponds to reduction of Cu^+ to Cu^0, respectively.

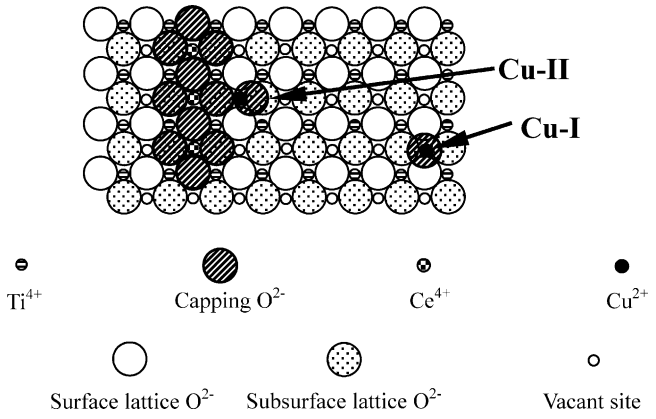

Fig. 14. The schematic diagram for the incorporated Cu^{2+} ions in the surface vacant sites on the (0 0 1) plane of ceria-modified TiO_2 (anatase).

Fig. 12 shows the TPR profiles of *x*Cu–6Ce–Ti samples. Two peaks around 160 and 290 °C appear in all the three profiles, and which seems to suggest that, for these samples, two kinds of copper oxide species are the main ones. The reduction peaks around 290 °C present two characteristics, e.g. the shift of the peak to the higher temperature and the peak intensity becoming stronger with the increasing copper loading, which should be caused by the increasing amount of the formed crystalline CuO, signed as Cu–IV. The peaks at about 160 °C should be corresponding to the Cu–II species, i.e. the highly dispersed copper oxide species closely contacting with the dispersed ceria on TiO_2, and the amount of this species was calculated in Table 2. Noting that, for the reduction temperature around 160 °C, the profile shape, the peak temperature and the peak intensity did not vary evidently with copper oxide loadings, which suggest that Cu–II species, not Cu–I species, should be the predominant copper oxide in these samples. This result seems easily to be understood because of the relatively more dispersed ceria species on the surface of TiO_2 in these samples (compared with *x*Cu–3Ce–Ti samples) and the increase of the connection possibility of the dispersed copper oxide species with the dispersed ceria species, as shown in Fig. 14.

Fig. 13 shows the TPR profiles of the *x*Cu–40Ce–Ti samples, and the CuO/CeO_2 sample (4.76 Cu^{2+} ions/nm^2 CeO_2) was used as the reference. The results indicate that the profile-shape and the reduction peak temperatures are basically similar, and which suggested that there are some copper species with the same states existing in all the samples. Considering the fact that the full surface of TiO_2 could be covered by the dispersed ceria and the formed crystalline ceria existed in all the *x*Cu–40Ce–Ti samples, it seems reasonable to suggest that the dispersed copper oxide species on the surface ceria should be the common one in all the samples, e.g. CuO/CeO_2. And this proposal should be further supported by the comparison of the TPR results of

the 4Cu–40Ce–Ti and CuO/CeO_2 samples, i.e. the reduction temperature peaks in profiles Fig. 13(a) and (b) are almost the same. In addition, the intensities of the reduction peaks gradually increase as the increasing copper loading, and this should be resulted from the increasing amount of the crystalline copper oxide formed in the samples, as proved by XRD. In fact, for all the three *x*Cu–40Ce–Ti samples, all vacant sites on the surface of TiO_2 have been occupied by the dispersed ceria species and the extra ceria would form crystalline CeO_2, and consequently, the three samples can be approximately regarded as the composition of two systems, CuO/CeO_2 and CeO_2/TiO_2. Furthermore, it seems to suggest that, for $CuO/CeO_2/TiO_2$ catalysts, the excess ceria would form the crystalline ceria, which would result in the dispersion of copper oxide on its surface and reduce the use of ceria as a promoter as well as the TiO_2 as the support in the ceria-modified catalysts. Noteworthy, this result is different from that for the $CuO/WO_3/CeO_2$ system reported previously [37], in which copper oxide could continuously disperse on the surface of tungsten covered ceria particles. As to the hazy shoulder peaks appeared in the TPR profiles (c) and (d), as well as the possible reduction peaks covered in the broad profiles, a detailed description and discussion will be presented elsewhere.

3.4. "NO + CO" reaction activity of the Cu–Ce–Ti catalysts in different compositions and temperatures

Table 3 shows the NO conversion and the N_2 selectivity of the Cu–Ce–Ti samples at 200 °C for NO + CO reaction. For comparison, reactivity data of CuO/CeO_2 and CuO/TiO_2 catalysts are also listed. The results show that the NO conversion increases in the order: 4Cu–6Ce–Ti < CuO/TiO_2 < CuO/CeO_2 ≈ 4Cu–40Ce–Ti. For the 4Cu–6Ce–Ti sample, the catalyst shows poor activity, which is lower than that in CuO/TiO_2 catalyst; while for the 4Cu–40Ce–Ti sample with high ceria loading, the catalyst shows high activity, which is close to that of CuO/CeO_2. The results suggested that, for the low ceria-modified TiO_2, the existence of dispersed ceria on the TiO_2 support lowers the activity for NO + CO reaction, and which is contrast with the results shown in Cu–Ce–Al catalyst [35], i.e. for the lower ceria-modified γ-Al_2O_3 catalyst, the activity is higher than that of CuO/γ-Al_2O_3.

As reported elsewhere, for metal-oxide catalysts, the state of the surface oxygen species will play an important role in

Table 3
For NO + CO reaction, NO conversion and the N_2 selectivity of the Cu–Ce–Ti, CuO/TiO_2 and CuO/CeO_2 samples at 200 °C, reaction time 1 h

Sample number	4Cu–40Ce–Ti	4Cu–6Ce–Ti	8Cu–Ti	4Cu–Ce
NO conversion (%)	100	0	40.6	100
N_2 selectivity (%)	94.1	–	38.9	100

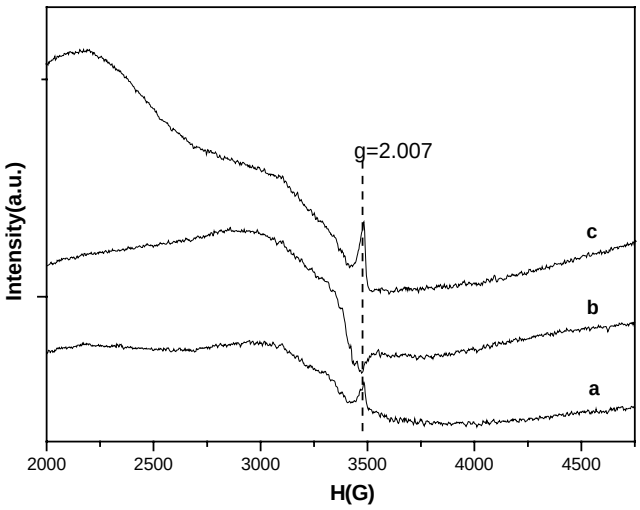

Fig. 15. ESR results at room temperature: (a) CuO/TiO_2; (b) CuO/CeO_2; (c) 4Cu–6Ce–Ti.

oxidation reactions [38]. To obtain further understanding of the influence of dispersed ceria on the surface of TiO_2, ESR results of the surface oxygen species about 4Cu–6Ce–Ti, CuO/CeO_2 (in which, 2.41 Cu^{2+} ions/nm^2 CeO_2) and CuO/TiO_2 (in which, 4.94 Cu^{2+} ions/nm^2 TiO_2) have been recorded and shown in Fig. 15. The ESR signal at $g = 2.007$ can be observed for all the three catalysts, which should be attributed to the adsorbed O_2^- species on the surface of catalysts [39,40]. However, the directions of the signal are different, i.e. the signals of 4Cu–6Ce–Ti and CuO/TiO_2 are opposite to that of CuO/CeO_2, which seems to suggest that the states of surface O_2^- species should be different in these samples and the surface O_2^- species with the negative direction at $g = 2.007$ might be the active ones in the NO + CO reaction.

Fig. 16 presents the relationship between the NO conversion, the N_2 selectivity of 4Cu–6Ce–Ti and CuO/TiO_2 samples and reaction temperatures. The results show that the N_2 selectivity and the NO conversion increases with the increasing temperature, except the decreasing NO conversion of CuO/TiO_2 sample at the reaction temperature from 300 to 400 °C. In addition, for the 4Cu–6Ce–Ti catalyst, the color of the catalysts has changed from gray to dark, as well as slightly red after used at 400 °C, which implies that the reduction of surface copper species to Cu^0 occurs during the reaction. As discussed elsewhere [41], the nature of the different behavior of the catalysts should be related to the different reaction mechanism at different reaction conditions.

To get more understanding about the behaviors of *x*Cu–*y*Ce–Ti samples in NO + CO reaction, the variation of NO conversions and/or N_2 selectivity at different reaction time and temperatures have also been explored (the results have not shown in this paper). However, it seems difficult to explain the results shown in our experiment for the time being, because of the complexity in

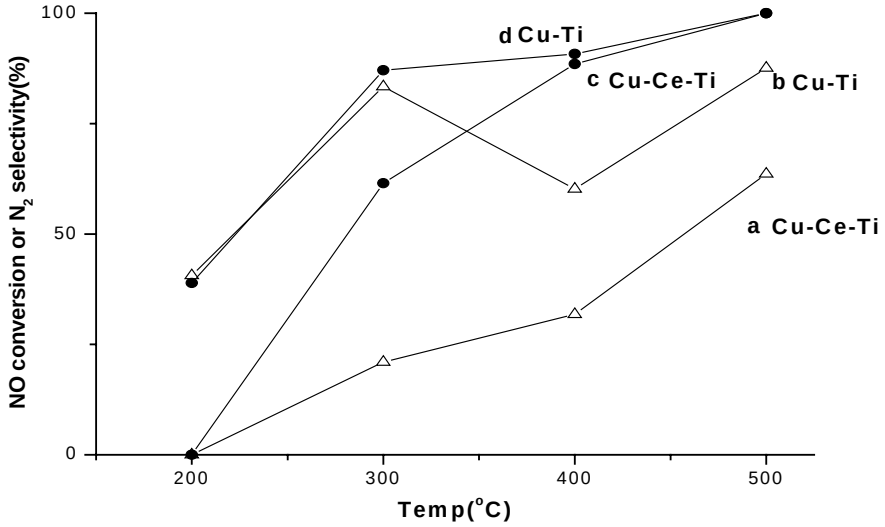

Fig. 16. Relationship between the NO conversions (□), the N_2 selectivity (●) of 4Cu–6Ce–Ti and CuO/TiO_2 samples and reaction temperature: (a) the NO conversion of 4Cu–6Ce–Ti; (b) the NO conversion of Cu–Ti; (c) the N_2 selectivity of 4Cu–6Ce–Ti; (d) the N_2 selectivity of Cu–Ti.

this system, and a further study is being carried out in our laboratory.

4. Conclusion

1. From XRD and Raman results, the DC of ceria on the surface of TiO_2 is about 6.98 Ce^{4+} ions/nm^2 TiO_2, which is basically in agreement with the value predicted by the incorporation model.
2. The dispersion of copper oxide and the state of the dispersed copper oxide species on ceria-modified TiO_2 closely depend on the ceria loading amounts. For the samples with low ceria loading amounts, the dispersion of copper oxide decreases with the ceria loading amounts, while when the ceria loading amounts are beyond 6.98 Ce^{4+} ions/nm^2 TiO_2, the dispersion of copper oxide increases with the formation of ceria particles.
3. TPR results show that, for the samples with ceria loading amounts lower than its DC, two kinds of dispersed copper oxide species are probably formed, e.g. Cu–I and Cu–II, which is due to the connection or not connection of dispersed copper oxide species with the dispersed ceria species; as the ceria loading amounts are highly beyond the DC, $CuO/CeO_2/TiO_2$ systems can be regarded as the composition of CuO/CeO_2 and CeO_2/TiO_2.
4. In NO + CO reactions, the NO conversion increases as: 4Cu–6Ce–Ti < CuO/TiO_2 < CuO/CeO_2 ≈ 4Cu–40Ce–Ti. For 4Cu–6Ce–Ti sample, the existence of dispersed ceria on TiO_2 would restrain the catalytic activity of copper oxide species; and for 4Cu–40Ce–Ti sample, the catalyst would be approximately regarded as the composition of two systems, CuO/CeO_2 and CeO_2/TiO_2, and result in a similar catalytic activity to CuO/CeO_2.

Acknowledgements

The financial supports of the Science and Technology Cooperation Item of Jiang-su Province, China (No. BG2001038) and the Special of Foundation for the Doctor-subject of China (No. 20030284002) are gratefully acknowledged.

References

[1] H.P. Boehm, H. Knozinger, in: J.R. Anderson, M. Boudart (Eds.), Analysis, Science and Technology, vol. 4, Springer-Verlag, West Berlin, 1983, p. 39.
[2] Yu.I. Yermakov, B.N. Kuznetsov, V.A. Zakharov, Analysis by Supported Complexes, Elsevier, Amsterdam, 1981.
[3] B. Delmon, M. Houalla, in: B. Delmon, P. Grange, P.A. Jacobs, G. Poncelet (Eds.), Preparation of Catalysts II, Elsevier, Amsterdam, 1979, p. 447.
[4] H. Knozinger, E. Taglauer, in: J.J. Spivey, S.K. Agarwal (Eds.), Catalysis, vol. 10, A Specialist Periodical Report, The Royal Society of Chemistry, London, 1993, p. 1.
[5] F.E. Massoth, Adv. Catal. 27 (1978) 265.
[6] L. Dong, Y. Hu, F. Xu, D. Lu, B. Xu, Z. Hu, Y. Chen, J. Phys. Chem. 104 (2000) 78.
[7] L. Dong, Y. Hu, M. Shen, T. Jin, J. Wang, W. Ding, Y. Chen, Chem. Mater. 13 (2001) 4227.
[8] S. Matsuda, A. Kato, Appl. Catal. 8 (1983) 149.
[9] H.B. Jones, R. Smith, US Patent 4 206 038, 1980.
[10] Y. Okamoto, A. Maezawa, T. Imamaka, J. Catal. 120 (1989) 29.
[11] M.A. Reiche, E. Ortelli, A. Baiker, Appl. Catal. B 23 (1999) 187.
[12] J.P. Dunn, P.R. Koppula, H.G. Stenger, I.E. Wachs, Appl. Catal. B 19 (1998) 103.
[13] Y.C. Liu, G.L. Griffin, S.S. Chan, I.E. Wachs, J. Catal. 94 (1985) 108.
[14] K.Y.S. Ng, E. Gulari, J. Catal. 92 (1983) 340.
[15] J. Kašpar, P. Fornasiero, M. Graziani, Catal. Today 50 (1999) 285.
[16] R.T. Rewick, H. Wise, J. Catal. 40 (1975) 301.

[17] F. Boccuzzi, E. Guglielminotti, G. Martra, G. Cerrato, J. Catal. 146 (1994) 449.
[18] M.C. Wu, D.W. Goodman, J. Phys. Chem. 98 (1994) 9874.
[19] H. Knozinger, Adv. Catal. 25 (1976) 184.
[20] P.Y. Lin, M. Skoglundh, L. Lowendahl, J.E. Otterstedt, L. Dahl, K. Jansson, M. Nygren, Appl. Catal. B 6 (1995) 237.
[21] J.W. London, A.T. Bell, J. Catal. 31 (1973) 96.
[22] R. Hierl, H.P. Urbach, H. Knozinger, J. Chem. Soc., Faraday Trans. 88 (1992) 355.
[23] A.R. Balkenede, H. den Daas, M. Huisman, O.L.J. Gijzeman, J.W. Geus, Appl. Surf. Sci. 47 (1991) 341.
[24] P. Larsson, A. Andersson, L.R. Wallenberg, B. Svensson, J. Catal. 163 (1996) 279.
[25] P. Larsson, A. Andersson, J. Catal. 179 (1998) 72.
[26] W. Li, R. Yang, Energy Fuel 11 (1997) 428.
[27] B. Xu, L. Dong, Y. Chen, J. Chem. Soc., Faraday Trans. 94 (1998) 1905.
[28] Y.C. Xie, Y.Q. Tang, Adv. Catal. 37 (1990) 1.
[29] B. Xu, L. Dong, Y.N. Fan, Y. Chen, J. Catal. 193 (2000) 88.
[30] Y. Chen, L.F. Zhang, Catal. Lett. 12 (1992) 51.
[31] L. Dong, Y.S. Jing, Y. Chen, Sci. China, Ser. B 40 (1997) 24.
[32] D. Brigs, M.P. Seah (Eds.), Practical Surface Analysis by Auger and X-ray Photoelectron Spectroscopy, Wiley, New York, 1983.
[33] P. Zimmer, A. Tschope, R. Birringer, J. Catal. 205 (2002) 339.
[34] F. Pinna, T. Fantinel, G. Strukul, A. Benedetti, N. Pernicone, Appl. Catal. A 149 (1997) 341.
[35] K. Hadjiivanov, M. Mihaylov, D. Klissurski, P. Stefanov, N. Abadjieva, E. Vassileva, L. Mintchev, J. Catal. 185 (1999) 314.
[36] P. Larsson, A. Andersson, Appl. Catal. B 24 (2000) 175.
[37] L. Dong, Y.H. Hu, F. Xu, D. Lu, B. Xu, Z. Hu, Y. Chen, J. Phys. Chem. 104 (2000) 78.
[38] P.J. Gellings, H.J.M. Bouwmeester, Catal. Today 58 (2000) 1.
[39] D. Dvoranova, V. Brezova, M. Mazur, M.A. Malati, Appl. Catal. B 37 (2002) 91.
[40] J. Soria, A. Martinez-Arias, J.C. Conesa, J. Chem. Soc., Faraday Trans. 91 (1995) 1669.
[41] G. Centi, S. Perathoner, Appl. Catal. A 132 (1995) 179.